Exploiting the Kinematic Redundancy of a (6+3)-DoF Parallel Manipulator to Produce Unlimited Rotation of the Platform

Arda Yiğit, David Breton, Clément Gosselin

Exploiting the Kinematic Redundancy of a (6+3)-DoF Parallel Manipulator to Produce Unlimited Rotation of the Platform

Arda Yiğit*

Département de génie mécanique
Université Laval
Québec, QC G1V 0A6, Canada
Email: arda.yigit.1@ulaval.ca

David Breton

Département de génie mécanique
Université Laval
Québec, QC G1V 0A6, Canada
Email: david.breton.2@ulaval.ca

Clément Gosselin
Fellow ASME
Département de génie mécanique
Université Laval
Québec, QC G1V 0A6, Canada
Email: gosselin@gmc.ulaval.ca

Mechanical interference and singularities within the reachable workspace often restrict the orientational workspace of parallel robots. Introducing kinematic redundancy can alleviate this limitation. This paper discusses the possibility to produce unlimited rotation of the platform of a tripedal $(6+3)$-degree-of-freedom kinematically redundant parallel robot. The articulated platform of such a robot has three degrees of mobility. The platforms considered here are planar linkages that contain either revolute or prismatic joints. It is shown that at least two revolute joints are required to produce unlimited rotation with appropriate design and initial configuration, while the platforms with two prismatic joints cannot produce such rotations without crossing a singularity.

1 INTRODUCTION

Mechanical interference and type II (or parallel) singularities within the reachable workspace often limit the orientational capabilities of parallel robots. A typical example is the tilt angle of a Gough-Stewart platform which is limited to approximately $45°$ [1]. While the size of the translational workspace of a robot can be increased by scaling up the geometric parameters, the orientational workspace is scale invariant. In particular, designing a parallel robot capable of producing an unlimited rotation of the platform is a challenging problem. Existing solutions are lower mobility parallel manipulators, often providing Schöenflies motions (motions of the SCARA robot). Schöenflies motion parallel robots can achieve unlimited rotation by using kinematic redundancy [2]. Nonredundant designs also exist, but suffer from a limited workspace [3] or use motion transformation, which deteriorates the efficiency and the stiffness [4].

Typical applications of parallel robots usually do not require large ranges of orientations. However, significant orientational capabilities may be necessary for manipulation or advanced grasping techniques (e.g., scooping [5]). Introducing kinematic redundancy can alleviate this limitation (see, for instance, [6, 7, 8, 9, 10]). The reader may refer to recent reviews on kinematic redundancy for a better overview [11, 1]. As notable examples, kinematic redundancy was used (i) on a planar robot to obtain unlimited rotation and also to actuate a gripper at the end-effector using the redundant degree of freedom (DoF) [6] and (ii) on a spatial hybrid parallel $(6+3)$-DoF robot with very large — but not unlimited, because of mechanical

*Corresponding author.

interference — orientational workspace and a remotely operated gripper [10]. Other 3-DoF planar platforms that can be used on the $(6+3)$-DoF robot mentioned previously were also studied [12].

The redundant DoFs must be controlled to avoid singular configurations [13]. Singularity avoidance on robots is a well-known topic that has been researched for several decades. Yoshikawa introduces and uses the manipulability measure in a multi-objective optimization problem for the trajectory control of a robot while avoiding singularities [14]. Klein and Blaho compare different dexterity measures for the design and control of manipulators with kinematic redundancy [15]: the manipulability measure, the condition number, the minimum singular value and the joint range availability [16]. Voglewede and Ebert-Uphoff give a general form for a singularity index that is equivalent to the solution of a generalized eigenvalue problem [17]. The generalized eigenvalue problem can be formulated such that it has a physical meaning. The physical meaning can be related to different quantities, such as the lowest natural frequency of the manipulator [17], the power developed by each leg [18, 19] or the potential energy associated to the stiffness of each actuator. Performance indices based on the static behaviour of a parallel manipulator have also been proposed [20, 21].

In the above-mentioned work by Wen et al. [10], the authors show that all type II singularities can be avoided by restricting the redundant joint angles to $\pm 60^\circ$ if the proximal links (with respect to the platform) are short enough to avoid any mutual intersection. While convenient, this method is nevertheless restrictive since (i) it prevents large ranges of motion and (ii) it limits the moment of the force generated by the leg that is proportional to the length of the proximal link.

In this work, we revisit the $(6+3)$-DoF tripedal parallel robots with planar configurable platforms proposed in [10, 12] in order to synthesize kinematic architectures that can perform unlimited rotation at the end-effector. Here, unlimited rotation means that the platform is able to rotate for any number of turns about some axis. To the best of our knowledge, this work presents the first 6-DoF parallel robot that can achieve unlimited torsion. Each leg of the parallel robot consists of a 3-DoF robot controlling the Cartesian position of its end-effector. The legs are attached to the configurable platform through spherical joints. The platform has three degrees of mobility obtained by combining revolute and prismatic joints. First, the kinematic modelling of a platform with three revolute joints is presented (Section 2) and the singularities are analyzed (Section 3). Then, two different singularity indices are compared (Section 4). A path planning approach is presented in order to perform an unlimited rotation of the platform without crossing any singularity, assuming that one of the degrees of mobility of the platform is constrained (Section 5). The feasibility of the unlimited rotation is then discussed (Section 6). The influence of some geometric parameters is analyzed in order to guide the design of the platform (Section 7). Finally, two other platforms are explored, one with two revolute joints and one prismatic joint, the other one with one revolute joint and two prismatic joints (Section 8). The video accompanying the paper illustrates a remotely actuated gripper with unlimited rotation (https://youtu.be/D5txxesP51w).

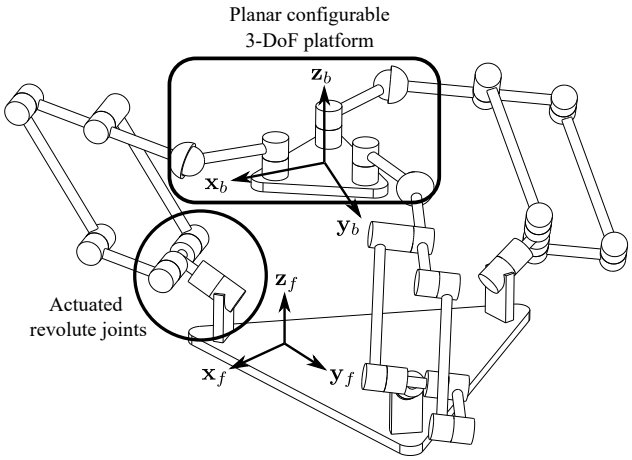

Fig. 1. Hybrid $(6+3)$-DoF robot (adapted from Wen et al. [10]). The actuated joints are highlighted in one of the legs.

2 MODELLING

2.1 Parameterization

Figure 1 (adapted from [10]) illustrates a $(6+3)$-DoF hybrid parallel robot. According to the nomenclature introduced by Gosselin and Schreiber in [7], the extra three DoFs correspond to the possible reorientation (or repositioning) of the links connecting the legs to the end-effector. Each of the three legs includes a fixed actuated revolute joint on which a planar five-bar linkage actuated by two base joints is mounted. The end of each leg consists of a passive spherical joint and the platform includes three passive revolute joints with parallel axes. Each leg includes three actuators located near the base. A fixed reference frame $\mathcal{R}_f = (O, \boldsymbol{x}_f, \boldsymbol{y}_f, \boldsymbol{z}_f)$ is attached to the base of the robot and a mobile reference frame $\mathcal{R}_b = (P, \boldsymbol{x}_b, \boldsymbol{y}_b, \boldsymbol{z}_b)$ is attached to the platform such that vector $\boldsymbol{z}_b$ is normal to the planar platform.

Figure 2 shows some geometric parameters of the planar platform. The platform is equipped with three revolute joints forming the vertices of a triangle. The posi-

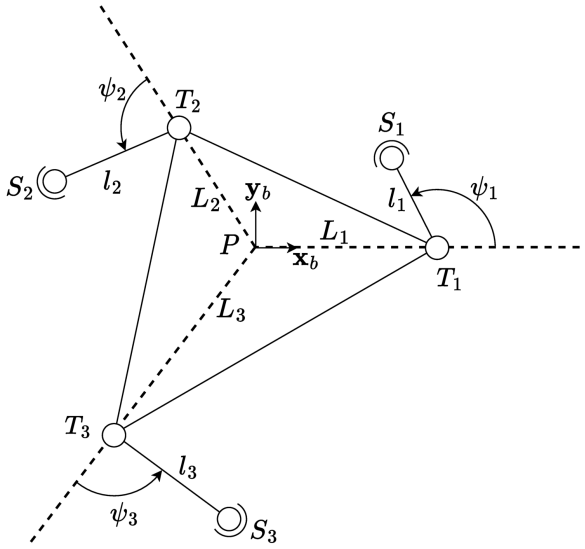

Fig. 2. Parameterization of the platform.

tion vector of vertex T_i in $\mathcal{R}_b$ is noted $\boldsymbol{t}_i$. The norm of $\boldsymbol{t}_i$ and its orientation angle with respect to $\boldsymbol{x}_b$ are noted respectively L_i and ϕ_i. With no loss of generality, it is assumed that $\phi_1 = 0$. A spherical joint of centre S_i is attached to the revolute joint at T_i through a link of length l_i. These spherical joints correspond to the end-effector of each leg of the tripedal parallel robot. The position of S_i in $\mathcal{R}_b$ is noted $\boldsymbol{s}_i$, and we define $\boldsymbol{u}_i = \boldsymbol{s}_i - \boldsymbol{t}_i$. The angle from $\boldsymbol{t}_i$ to $\boldsymbol{u}_i$ is noted ψ_i. The position of the moving frame $\mathcal{R}_b$ with respect to a fixed base frame $\mathcal{R}_f$ is noted $\boldsymbol{p}$, its orientation with respect to $\mathcal{R}_f$ is given by matrix $\boldsymbol{Q}$ and its angular velocity is noted $\boldsymbol{\omega}$.

2.2 Jacobian Matrices

The Jacobian matrices $\boldsymbol{J}$ and $\boldsymbol{K}$ describe the relationship between the end-effector velocities $\boldsymbol{v} = [\dot{\boldsymbol{p}}^T \quad \boldsymbol{\omega}^T]^T$ and the actuated joint velocities $\dot{\boldsymbol{s}} = [\dot{\boldsymbol{s}}_1^T \ \dot{\boldsymbol{s}}_2^T \ \dot{\boldsymbol{s}}_3^T]^T$:

$$\boldsymbol{J}\boldsymbol{v} = \boldsymbol{K}\dot{\boldsymbol{s}} \tag{1}$$

where $\dot{\boldsymbol{s}}_i$ is the three-dimensional vector containing the actuated joint velocities of the i-th leg of the robot.

In the following, we use screw theory to find the expressions of $\boldsymbol{J}$ and $\boldsymbol{K}$. Let $\xi_{EE} = [\boldsymbol{\omega}^T \ (\dot{\boldsymbol{p}} + \boldsymbol{p} \times \boldsymbol{\omega})^T]^T_O$ be the twist of the platform expressed with respect to the base frame origin O, ξ_{P_i} the twist of the i-th leg, ξ_{S_i} the twist of the spherical joint at S_i and ξ_{T_i} the twist of the revolute joint at T_i. Then,

$$\xi_{EE} = \xi_{P_i} + \xi_{S_i} + \xi_{T_i}. \tag{2}$$

Let $\xi_{S_i,\boldsymbol{u}_i}$ be a zero-pitch twist of line $(S_i, \boldsymbol{u}_i)$ and amplitude $\|\boldsymbol{u}_i\| = l_i$. Then, $\xi_{S_i,\boldsymbol{u}_i}$ is reciprocal to ξ_{S_i} and ξ_{T_i}, and

$$\xi_{S_i,\boldsymbol{u}_i} \cdot \xi_{EE} = \xi_{S_i,\boldsymbol{u}_i} \cdot \xi_{P_i} \tag{3}$$

which gives

$$\boldsymbol{u}_i{}^T\dot{\boldsymbol{p}} + (\boldsymbol{t}_i \times \boldsymbol{u}_i)^T\boldsymbol{\omega} = \boldsymbol{u}_i{}^T\dot{\boldsymbol{s}}_i. \tag{4}$$

Let $\xi_{S_i,\boldsymbol{z}_b}$ be a zero-pitch twist of line $(S_i, \boldsymbol{z}_b)$ and amplitude $\|\boldsymbol{z}_b\| = 1$. Then, $\xi_{S_i,\boldsymbol{z}_b}$ is reciprocal to ξ_{S_i} and ξ_{T_i} (since the axis of the revolute joint at T_i is also in the direction of $\boldsymbol{z}_b$) and

$$\xi_{S_i,\boldsymbol{z}_b} \cdot \xi_{EE} = \xi_{S_i,\boldsymbol{z}_b} \cdot \xi_{P_i} \tag{5}$$

which gives

$$\boldsymbol{z}_b{}^T\dot{\boldsymbol{p}} + (\boldsymbol{s}_i \times \boldsymbol{z}_b)^T\boldsymbol{\omega} = \boldsymbol{z}_b{}^T\dot{\boldsymbol{s}}_i. \tag{6}$$

Combining (4) and (6) yields the expressions of $\boldsymbol{J}$ and $\boldsymbol{K}$

$$\begin{bmatrix} \boldsymbol{u}_1{}^T & (\boldsymbol{t}_1 \times \boldsymbol{u}_1)^T \\ \boldsymbol{u}_2{}^T & (\boldsymbol{t}_2 \times \boldsymbol{u}_2)^T \\ \boldsymbol{u}_3{}^T & (\boldsymbol{t}_3 \times \boldsymbol{u}_3)^T \\ \boldsymbol{z}_b{}^T & (\boldsymbol{s}_1 \times \boldsymbol{z}_b)^T \\ \boldsymbol{z}_b{}^T & (\boldsymbol{s}_2 \times \boldsymbol{z}_b)^T \\ \boldsymbol{z}_b{}^T & (\boldsymbol{s}_3 \times \boldsymbol{z}_b)^T \end{bmatrix} \begin{bmatrix} \dot{\boldsymbol{p}} \\ \boldsymbol{\omega} \end{bmatrix} = \begin{bmatrix} \boldsymbol{u}_1{}^T & \boldsymbol{0}^T & \boldsymbol{0}^T \\ \boldsymbol{0}^T & \boldsymbol{u}_2{}^T & \boldsymbol{0}^T \\ \boldsymbol{0}^T & \boldsymbol{0}^T & \boldsymbol{u}_3{}^T \\ \boldsymbol{z}_b{}^T & \boldsymbol{0}^T & \boldsymbol{0}^T \\ \boldsymbol{0}^T & \boldsymbol{z}_b{}^T & \boldsymbol{0}^T \\ \boldsymbol{0}^T & \boldsymbol{0}^T & \boldsymbol{z}_b{}^T \end{bmatrix} \begin{bmatrix} \dot{\boldsymbol{s}}_1 \\ \dot{\boldsymbol{s}}_2 \\ \dot{\boldsymbol{s}}_3 \end{bmatrix}, \tag{7}$$

where $\boldsymbol{0}^T$ stands for the zero three-dimensional line vector.

3 SINGULARITY ANALYSIS

Singularities restrict the orientational workspace of parallel robots. Their analysis is necessary in order to enable unlimited rotation of the platform.

3.1 Type I Singularities

The robot is in a type I singularity if the Jacobian matrix $\boldsymbol{K}$ is rank-deficient: $\mathrm{rank}(\boldsymbol{K}) < 6$. Since $\boldsymbol{u}_i$ and $\boldsymbol{z}_b$ are always linearly independent ($\boldsymbol{u}_i$ has no component along the $\boldsymbol{z}_b$ axis), matrix $\boldsymbol{K}$ is trivially full row rank. Therefore, the platform has no type I singularity.

3.2 Type II Singularities

The robot is in a type II singularity if the Jacobian matrix $\boldsymbol{J}$ is singular, i.e., $\det(\boldsymbol{J}) = 0$. By noticing that (i) $\boldsymbol{u}_i$ and $\boldsymbol{s}_i \times \boldsymbol{z}_b$ have no component along $\boldsymbol{z}_b$ and (ii) $\boldsymbol{t}_i \times \boldsymbol{u}_i$ is collinear to $\boldsymbol{z}_b$, the singularity condition can be written as the following: $\boldsymbol{J}$ is singular if and only if either $\boldsymbol{J}_z$ or $\boldsymbol{J}_u$ is singular, with

$$\boldsymbol{J}_z = \begin{bmatrix} 1 & (\boldsymbol{s}_1 \times \boldsymbol{z}_b)^T \boldsymbol{x}_b & (\boldsymbol{s}_1 \times \boldsymbol{z}_b)^T \boldsymbol{y}_b \\ 1 & (\boldsymbol{s}_2 \times \boldsymbol{z}_b)^T \boldsymbol{x}_b & (\boldsymbol{s}_2 \times \boldsymbol{z}_b)^T \boldsymbol{y}_b \\ 1 & (\boldsymbol{s}_3 \times \boldsymbol{z}_b)^T \boldsymbol{x}_b & (\boldsymbol{s}_3 \times \boldsymbol{z}_b)^T \boldsymbol{y}_b \end{bmatrix} \tag{8}$$

and

$$\boldsymbol{J}_u = \begin{bmatrix} \boldsymbol{u}_1{}^T \boldsymbol{x}_b & \boldsymbol{u}_1{}^T \boldsymbol{y}_b & (\boldsymbol{t}_1 \times \boldsymbol{u}_1)^T \boldsymbol{z}_b \\ \boldsymbol{u}_2{}^T \boldsymbol{x}_b & \boldsymbol{u}_2{}^T \boldsymbol{y}_b & (\boldsymbol{t}_2 \times \boldsymbol{u}_2)^T \boldsymbol{z}_b \\ \boldsymbol{u}_3{}^T \boldsymbol{x}_b & \boldsymbol{u}_3{}^T \boldsymbol{y}_b & (\boldsymbol{t}_3 \times \boldsymbol{u}_3)^T \boldsymbol{z}_b \end{bmatrix}. \tag{9}$$

3.2.1 Determinant 1

Matrix $\boldsymbol{J}_z$ can be rewritten as

$$\boldsymbol{J}_z = \begin{bmatrix} 1 & \boldsymbol{s}_1{}^T \boldsymbol{y}_b & -\boldsymbol{s}_1{}^T \boldsymbol{x}_b \\ 1 & \boldsymbol{s}_2{}^T \boldsymbol{y}_b & -\boldsymbol{s}_2{}^T \boldsymbol{x}_b \\ 1 & \boldsymbol{s}_3{}^T \boldsymbol{y}_b & -\boldsymbol{s}_3{}^T \boldsymbol{x}_b \end{bmatrix}. \tag{10}$$

The Laplace expansion with respect to the first column yields

$$\begin{aligned} \det(\boldsymbol{J}_z) = \begin{vmatrix} \boldsymbol{s}_2{}^T \boldsymbol{x}_b & \boldsymbol{s}_2{}^T \boldsymbol{y}_b \\ \boldsymbol{s}_3{}^T \boldsymbol{x}_b & \boldsymbol{s}_3{}^T \boldsymbol{y}_b \end{vmatrix} - \begin{vmatrix} \boldsymbol{s}_1{}^T \boldsymbol{x}_b & \boldsymbol{s}_1{}^T \boldsymbol{y}_b \\ \boldsymbol{s}_3{}^T \boldsymbol{x}_b & \boldsymbol{s}_3{}^T \boldsymbol{y}_b \end{vmatrix} \\ + \begin{vmatrix} \boldsymbol{s}_1{}^T \boldsymbol{x}_b & \boldsymbol{s}_1{}^T \boldsymbol{y}_b \\ \boldsymbol{s}_2{}^T \boldsymbol{x}_b & \boldsymbol{s}_2{}^T \boldsymbol{y}_b \end{vmatrix} \end{aligned} \tag{11}$$

which is equivalent to

$$\det(\boldsymbol{J}_z) = [\boldsymbol{s}_1 \times \boldsymbol{s}_2 - \boldsymbol{s}_1 \times \boldsymbol{s}_3 + \boldsymbol{s}_2 \times \boldsymbol{s}_3]^T \boldsymbol{z}_b. \tag{12}$$

Grassmann line geometry gives a geometric interpretation: the singularities of matrix $\boldsymbol{J}_z$ correspond to the alignment of S_i [10]. As a consequence, matrix $\boldsymbol{J}_z$ cannot be singular if l_i is chosen small enough to prevent the alignment of joints S_i.

3.2.2 Determinant 2

After noticing that $(\boldsymbol{t}_i \times \boldsymbol{u}_i)^T \boldsymbol{z}_b = L_i l_i \sin\psi_i$, the Laplace expansion of $\boldsymbol{J}_u$ with respect to the third column yields

$$\begin{aligned} \det(\boldsymbol{J}_u) = [&L_1 l_1 \sin\psi_1 (\boldsymbol{u}_2 \times \boldsymbol{u}_3) \\ &- L_2 l_2 \sin\psi_2 (\boldsymbol{u}_1 \times \boldsymbol{u}_3) \\ &+ L_3 l_3 \sin\psi_3 (\boldsymbol{u}_1 \times \boldsymbol{u}_2)]^T \boldsymbol{z}_b. \end{aligned} \tag{13}$$

According to Grassmann line geometry, $\boldsymbol{J}_u$ is singular if and only if lines $(S_i, \boldsymbol{u}_i)$ have a common intersection or are parallel [10].

4 SINGULARITY INDEX

One possible approach to produce an unlimited rotation of the end-effector is to couple this rotation to one of the redundant links. For instance, if ψ_1 is performing an unlimited rotation and ψ_2 is constant, a singularity avoidance strategy is essential. Indeed, if ψ_3 is also constant, then at some point of the rotation of ψ_1, $\boldsymbol{J}_u$ will be singular. A possible solution is to choose a singularity index and control the orientation of the redundant links by maximizing the index. A singularity index is a positive semidefinite function $\mathcal{I}$ that vanishes only at singularities. Intuitively, it represents the "distance" to the singular configurations. However, there is no universal definition of the distance, since the Euclidean distance has no physical interpretation in most cases. In the following, we recall two singularity indices that are well known in the literature and compare their impact on joint forces for the manipulator considered here. These singularity indices are based on the Jacobian matrices from (1). These Jacobian matrices are independent from the pose (position and orientation) of the end-effector. This is clearly seen from (7). This is explained by the fact that the kinematics (1) are agnostic of the kinematics of the leg mechanism. Indeed, this result is generic (any serial or parallel manipulator that controls the Cartesian position of its end-effector can be used as a leg), but maintains the leg within a workspace far from singularities.

The analysis from Section 3 shows that type I singularities depend on the leg mechanisms and can even be completely avoided by using singularity-free 3-DoF robots. In order to stay as generic as possible, type I singularities are not considered here.

4.1 Maximum Actuated Joint Forces

In the neighbourhood of a type II singular configuration, the joint forces can become very large for a given external wrench applied to the platform. For a given external wrench $\boldsymbol{f}$ acting on the platform, the actuated joint

forces (or torques) $\boldsymbol{f}_j$ can be obtained using the principle of virtual work as

$$\boldsymbol{f}_j = (\boldsymbol{J}^{-1}\boldsymbol{K})^T \boldsymbol{f}. \tag{14}$$

The singularity index based on the maximum actuated joint forces, noted $\mathcal{I}_n$, is defined as the inverse of the maximum value of the actuated joint forces for any external wrench in some set $\mathbb{F}$:

$$\frac{1}{\mathcal{I}_n} = \sup_{\boldsymbol{f}\in\mathbb{F}} \|(\boldsymbol{J}^{-1}\boldsymbol{K})^T \boldsymbol{f}\|_\infty. \tag{15}$$

If $\mathbb{F}$ can be written as the Cartesian product of six intervals centred at 0, that is, if there exists a diagonal matrix $\tilde{\boldsymbol{F}} \in \mathbb{R}^{6\times 6}$ such that $\mathbb{F} = \{\tilde{\boldsymbol{F}}\boldsymbol{u},\ \|\boldsymbol{u}\|_\infty < 1\}$, then the singularity index $\mathcal{I}_n$ can be written as

$$\frac{1}{\mathcal{I}_n} = \sup_{\|\boldsymbol{u}\|_\infty \le 1} \|(\boldsymbol{J}^{-1}\boldsymbol{K})^T \tilde{\boldsymbol{F}}\boldsymbol{u}\|_\infty. \tag{16}$$

Hence, the reciprocal of the singularity index $\mathcal{I}_n$ becomes

$$\frac{1}{\mathcal{I}_n} = \|(\boldsymbol{J}^{-1}\boldsymbol{K})^T \tilde{\boldsymbol{F}}\|_\infty \tag{17}$$

which corresponds to the maximum absolute row sum of matrix $(\boldsymbol{J}^{-1}\boldsymbol{K})^T\tilde{\boldsymbol{F}}$. As a consequence, this singularity index is easy to compute numerically. This index is known as the infinity-norm-based kinematic sensitivity index proposed by Cardou et al. [22].

4.2 Determinant

Since type I singularities are not considered, the singularity index based on the determinant, noted $\mathcal{I}_d$, is

$$\mathcal{I}_d = |\det(\boldsymbol{J})|. \tag{18}$$

This index is positive semidefinite and vanishes only at singular configurations. However, its value is not directly related to the actuated joint forces. An increasing value of the determinant does not guarantee a decrease of the maximum actuated joint forces, even though a cross-correlation might be expected. Note that this index corresponds to Yoshikawa's manipulability measure [14].

An advantage of the index $\mathcal{I}_d$ compared to the index $\mathcal{I}_n$ is that $\mathcal{I}_d$ has a simple closed form, and so it may be possible to analytically determine if a feasible solution exists to the unlimited rotation problem.

4.3 Comparison

Figure 3 compares indices $\mathcal{I}_d$ and $\mathcal{I}_n$ for $\psi_1 \in [0;\ 2\pi[$ and for some selected platform loads. Angle ψ_2 is fixed to $\frac{\pi}{2}$ and angle ψ_3 is then selected in order to maximize the singularity index. Matrix $\tilde{\boldsymbol{F}}$ is diagonal, the entries are 1 for forces and 0.1 for moments. Four scenarios are considered for the comparison: (i) a unit force along the $\boldsymbol{x}_b$ direction, (ii) a unit force along the $\boldsymbol{z}_b$ direction, (iii) a unit torque around the $\boldsymbol{x}_b$ direction, (iv) a unit torque around the $\boldsymbol{z}_b$ direction. For each of these cases, the plots show the maximum actuator force obtained when maximizing $\mathcal{I}_d$ or $\mathcal{I}_n$. The platform considered here is similar to the one used in Wen et al. [10]. It is an equilateral triangle with $L_i = 0.08\,\mathrm{m}$ and the proximal links have the same length $l_i = 0.04\,\mathrm{m}$. Point P is the barycentre of the platform.

Two main observations can be made. First, with each of the indices, the maximum actuated joint forces are discontinuous, especially with index $\mathcal{I}_n$. Indeed, $\arg\max$ function that returns the argument of the function when it reaches its minimum is discontinuous. For example, if a function has two distinct local maxima, then an infinitesimal modification of this function may change the position of the global maximum. Therefore, the value of ψ_3 cannot be obtained by solely computing the maximum of the singularity index. A path planning approach is proposed in Section 5.

Second, it is not possible to conclude that one of the indices is better than the other, since the maximum actuator force is lower sometimes with one, sometimes with the other. This may seem counterintuitive since index $\mathcal{I}_n$ is designed to minimize the maximum actuated joint forces. However, this minimization is done in a worst-case scenario for a force belonging to $\mathbb{F}$. Hence, in cases other than the worst one, there is no reason for $\mathcal{I}_n$ to outdo $\mathcal{I}_d$. Yet, if $\mathbb{F}$ corresponds to a single wrench applied to the platform, then $\mathcal{I}_n$ will give the optimal solution if this wrench is indeed applied. This property may be useful in situations in which the external forces are already known, such as pick-and-place tasks with known objects.

The remaining of this paper considers $\mathcal{I}_d$ as the singularity index since (i) it can be written in a closed form and (ii) its maximum is less sensitive to small variations of the input ψ_1 (so there are fewer discontinuities).

5 PATH PLANNING

Consider the situation in which $\psi_1 \in [0;\ 2\pi[$ is performing a complete rotation and ψ_2 is constant. The feasibility of the unlimited rotation problem for ψ_2 varying in an interval $[\underline{\psi}_2, \overline{\psi}_2]$ is discussed in the Section 6. For now, consider the case where geometric parameters and

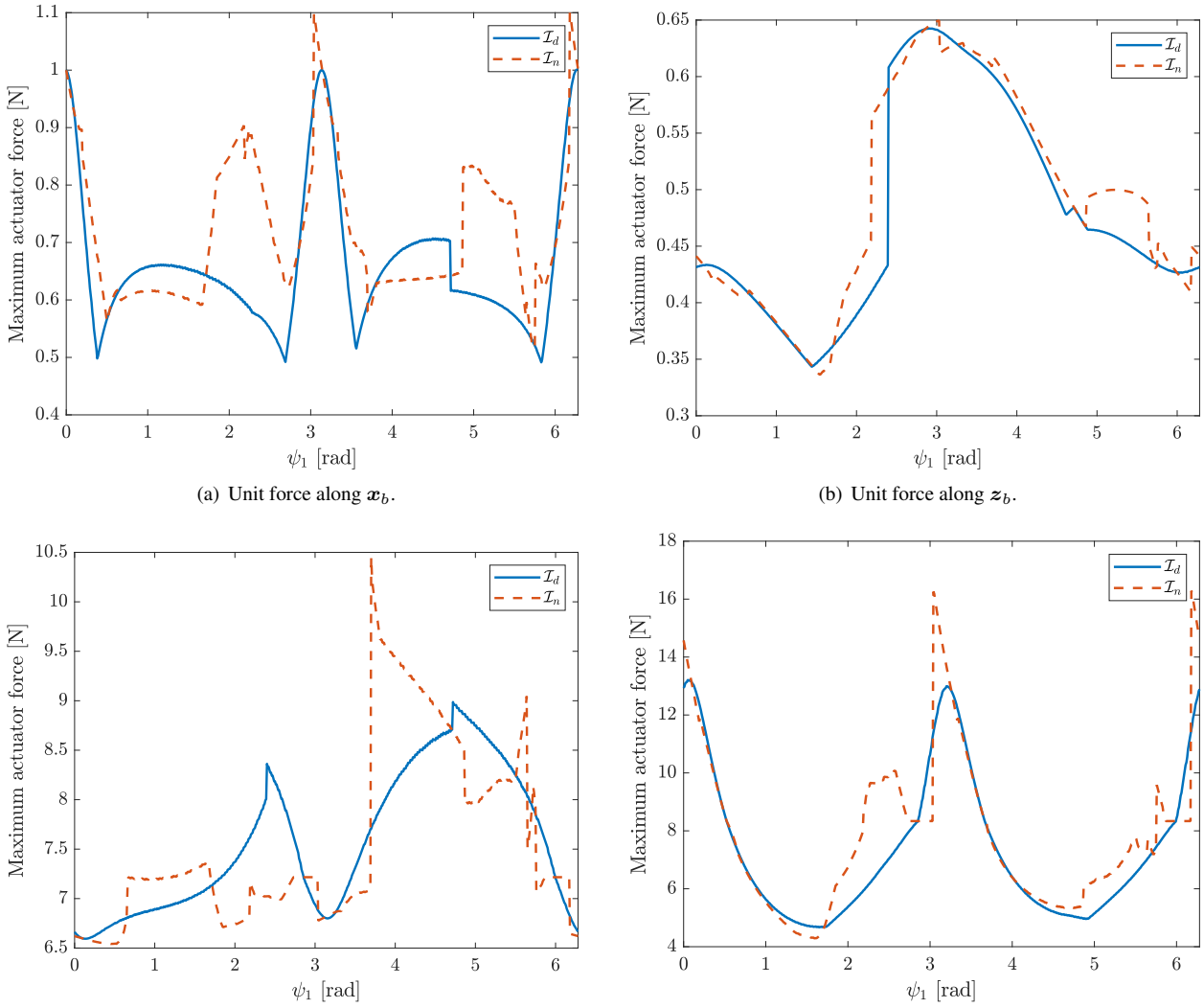

(a) Unit force along $\boldsymbol{x}_b$.

(b) Unit force along $\boldsymbol{z}_b$.

(c) Unit torque along $\boldsymbol{x}_b$.

(d) Unit torque along $\boldsymbol{z}_b$.

Fig. 3. Comparison of the maximum actuated joint force using each of the singularity indices.

ψ_2 are chosen such that the unlimited rotation problem is feasible and discuss how the path planning can be carried out. Note that it is not sufficient to find a value for ψ_3 for each value of ψ_1 to avoid singularities. This relation needs to be continuous, since ψ_3 cannot change instantaneously (it must be continuous).

The presented method can also be used if ψ_1 is constant and ψ_2 is varying. Therefore, it can be used for planning tasks requiring two DoFs, provided that ψ_1 and ψ_2 can be modified sequentially.

First, a simple case is presented for which a closed-form solution exists for the singularity-free path planning problem. Then, a solution is proposed for the general case.

5.1 Simplified Case

Some simplifying assumptions are made. The platform is assumed to be an equilateral triangle with circumradius $L = L_i$, and the proximal links have the same length $l = l_i$. If the length of the proximal links is such that $l < \frac{3}{4}L$, then $\boldsymbol{J}_z$ can never be singular [10]. Therefore, it is possible to consider only $\boldsymbol{J}_u$ for singularity avoidance. Equation (13) can be rewritten as

$$\det(\boldsymbol{J}_u) = lL(\boldsymbol{u}_1 \times \boldsymbol{u}_2)^T \boldsymbol{z}_b \sin\psi_3 + [lL(\sin\psi_1 \boldsymbol{u}_2 - \sin\psi_2 \boldsymbol{u}_1) \times \boldsymbol{u}_3]^T \boldsymbol{z}_b. \quad (19)$$

For given values of ψ_1 and ψ_2, the first term of

the expression is a harmonic function of ψ_3 of frequency $\frac{1}{2\pi}$. The second term is also a harmonic function of ψ_3 with the same frequency since $\|\boldsymbol{v}_1 \times \boldsymbol{v}_2\| = \|\boldsymbol{v}_1\|\|\boldsymbol{v}_2\||\sin(\boldsymbol{v}_1, \boldsymbol{v}_2)|$ where $\sin(\boldsymbol{v}_1, \boldsymbol{v}_2)$ is the sine of the angle between $\boldsymbol{v}_1$ and $\boldsymbol{v}_2$. The sum of two terms with same frequency is also a harmonic function (they are solution to the same linear ordinary differential equation). Hence, one can write

$$\det(\boldsymbol{J}_u) = c_1(\psi_1, \psi_2)\sin(\psi_3 + c_2(\psi_1, \psi_2)) \qquad (20)$$

where c_1 and c_2 are functions of angles ψ_1 and ψ_2 that can be readily obtained.

Therefore, if the unlimited rotation problem is feasible, then $\psi_3 = \frac{\pi}{2} - c_2(\psi_1, \psi_2)$ is a feasible solution. However, one may note that if ψ_2 is such that either T_1 or T_3 is aligned with T_2 and S_2, i.e., if $\psi_2 \in \{-\frac{5\pi}{6}, -\frac{\pi}{6}, \frac{\pi}{6}, \frac{5\pi}{6}\}$, then there is no feasible solution. Indeed, if the line $(T_2, \boldsymbol{u}_2)$ is coincident with either $(T_1, \boldsymbol{u}_1)$ or $(T_3, \boldsymbol{u}_3)$, the configuration is singular.

Figure 4 shows different solutions for $\psi_2 \in \left]\frac{\pi}{6}, \frac{5\pi}{6}\right[$ (Fig. 5.1) and $\psi_2 \in \left]-\frac{\pi}{6}, \frac{\pi}{6}\right[$ (Fig. 5.1). Cases where $\psi_2 \in \left]\frac{5\pi}{6}, \frac{7\pi}{6}\right[$ and $\psi_2 \in \left]\frac{7\pi}{6}, \frac{11\pi}{6}\right[$ are the same since the absolute value of the determinant of $\boldsymbol{J}_u$ is conserved if ψ_2 is shifted by π. A notable consequence is that if ψ_1 performs a complete rotation, so does ψ_3, and the direction of the rotation depends on the value of ψ_2.

5.2 General Case

Knowing ψ_1 and ψ_2, one may be tempted to select the value of ϕ_3 that maximizes the singularity index. However, as discussed previously in Section 4, the function $\arg\max$ is not continuous, and, thus, cannot be used here.

The approach implemented in this paper is similar to obstacle avoidance with artificial potential fields. Singular configurations correspond to repulsive sources and the target position to an attractive source.

When ψ_2 is fixed, the set of configurations $\{(\psi_1, \psi_3) \in \mathbb{R}^2\}$ define a toric space: the configurations are conserved under a 2π shift of the coordinates. Therefore, the distance between two configurations is not the Euclidean distance, but the shortest distance between two points on the surface of a torus.

Let $\mathbb{S}$ be the set of singular configurations. The repulsive potential V_{rep} at a point $\boldsymbol{q} = (\psi_1, \psi_3)$ is defined as

$$V_{rep}(\boldsymbol{q}) = \frac{1}{d_s(\boldsymbol{q}, \mathbb{S})} \qquad (21)$$

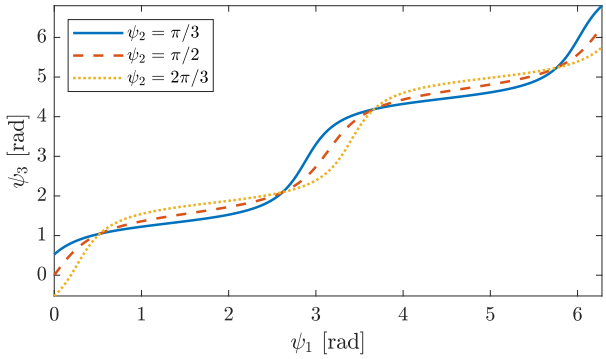

(a) Same direction

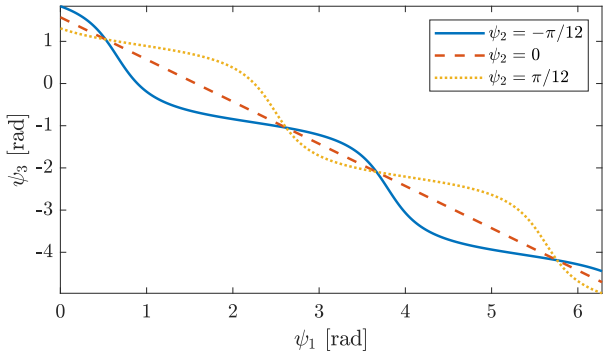

(b) Opposite direction

Fig. 4. Solutions to simple path planning.

where the function $d_s(\cdot, \mathbb{S})$ is the distance of the configuration $\boldsymbol{q}$ to the set $\mathbb{S}$. It corresponds to a singularity index. The attractive potential V_{att} is defined as

$$V_{att}(\boldsymbol{q}) = \|\boldsymbol{q} - \boldsymbol{q}_t\| \qquad (22)$$

with $\boldsymbol{q}_t$ the target configuration. In order to perform a complete rotation from an initial configuration $\boldsymbol{q}_0$, the target configuration is either $\boldsymbol{q}_t = \boldsymbol{q}_0 + (2\pi, -2\pi)$ or $\boldsymbol{q}_t = \boldsymbol{q}_0 + (2\pi, 2\pi)$, depending on the value of ψ_2. The total potential V is the sum of the repulsive and the attractive potentials: $V(\boldsymbol{q}) = V_{rep}(\boldsymbol{q}) + \lambda V_{att}(\boldsymbol{q})$, with $\lambda \geq 0$ a scaling coefficient.

Assuming a periodic sampling of ψ_1, the path from the initial configuration to the target configuration is obtained by gradient descent, namely

$$\Delta\psi_3 = -\varepsilon \frac{\partial V}{\partial \psi_3}(\psi_1, \psi_3). \qquad (23)$$

Applying the gradient descent algorithm to variable ψ_3 only prevents the algorithm from getting trapped in a local

minimum. Furthermore, for a given value of ψ_1, there is only one corresponding value of ψ_3.

This approach is tested in simulation with two repulsive potentials: the first one uses the singularity index $\mathcal{I}_d = \det(\boldsymbol{J})$ (case A) and the other uses the shortest distance to the singularities considering the toric geometry (case B). The platform is an equilateral triangle with $L_i = L = 8\times10^{-2}\,\mathrm{m}$ and $l_i = l = 7.3\times10^{-2}\,\mathrm{m}$. For the first case, the input increment is $\Delta\psi_1 = \frac{\pi}{36}$, the learning rate $\varepsilon = 0.11$ and the scaling coefficient $\lambda = 11.7L^3l^3$. For the second case, two parameters are modified: $\lambda = 5$ and $\varepsilon = 0.05$. Figure 5 shows the result of the path planning from the configuration $(\psi_1, \psi_3) = (0, 0)$ for $\psi_2 = \pi/3$ with both potentials. The colour map "batlow" is used to show the values of the potential [23]. The value of the potential V is saturated at 50. Solid lines represent the singularity locus and the dotted line represents the generated trajectory.

In this example, case B (using the shortest distance to $\mathbb{S}$) results in a smoother trajectory. The derivative of ψ_3 with respect to ψ_1 is shown in Fig. 6. Case A induces abrupt variations to ψ_3 to avoid singular configurations, more than fifteen times higher with respect to ψ_1 in the worst case. Furthermore, the lowest value reached by $\mathcal{I}_d$ is 34% lower with case A. Therefore, higher actuation forces may be required. Hence, using the shortest distance to $\mathbb{S}$ is preferred.

Note that not all nonsingular configurations are reachable from the initial position without crossing a singularity. Indeed, to perform a complete rotation, there are two distinct homotopy classes. The class of the chosen solution is defined by the initial configuration. Furthermore, for some initial nonsingular configurations, unlimited rotation is not feasible without modifying ψ_2 (e.g., $\psi_1 = 4\,\mathrm{rad}$ and $\psi_3 = 3\,\mathrm{rad}$, corresponding to the plus sign in Fig. 5).

The path generation could still fail because of local minima. More advanced techniques exist, such as modifying the potential to include virtual obstacles (i.e., generating a repulsive potential) [24] or implementing techniques that allow for escaping local minima [25]. Global path finding techniques could also be considered, since the dimension of the problem is low and the resolution could be carried out offline [26]. However, these are out of the scope of this paper.

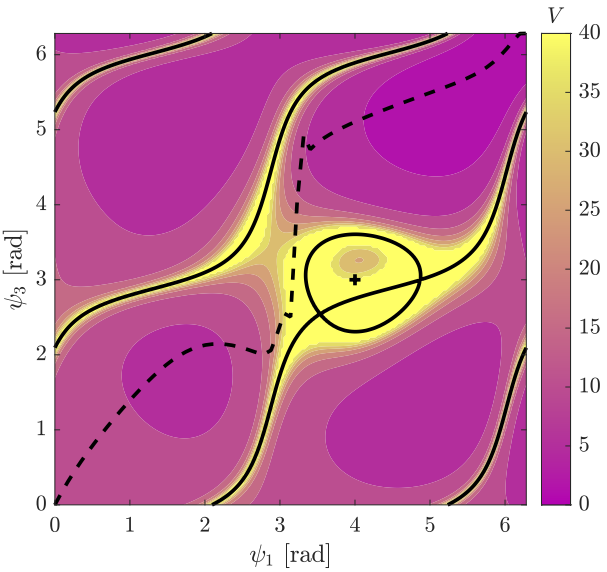

(a) Case A: using $\mathcal{I}_d$

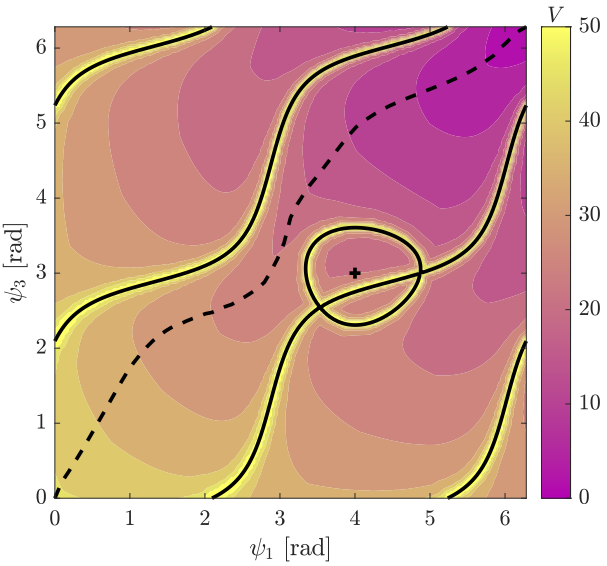

(b) Case B: using the shortest distance to $\mathbb{S}$

Fig. 5. Path planning with artificial potential fields. Solid lines are the singularity locus. The dotted line is the generated trajectory. The point with a plus sign is an initial configuration from which unlimited rotation is not feasible.

6 FEASIBILITY

The feasibility of unlimited rotation depends on the geometric parameters of the platform (L_i, l_i and ϕ_i) and the length and mean value of $[\underline{\psi}_2, \overline{\psi}_2]$, i.e., the interval of ψ_2. In the following, two conditions are presented. The first one is a geometric approach to avoid the singularity of matrix $\boldsymbol{J}_z$. The second one is a sufficient condition based on the path planning algorithm presented above in Section 5.

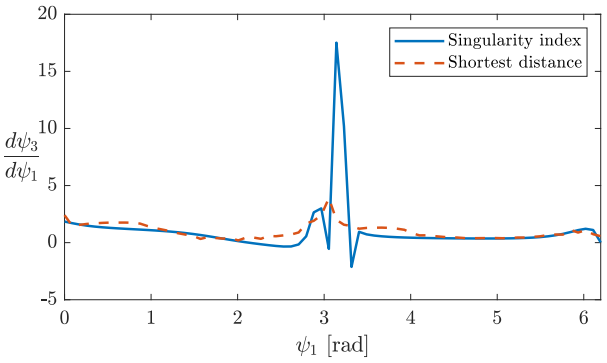

Fig. 6. Comparison of the rate of change of ψ_3 with respect to ψ_1 for each of the potentials.

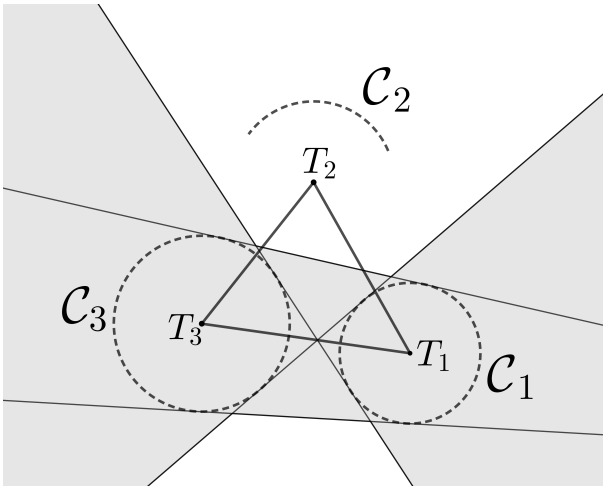

Fig. 7. Feasibility condition.

6.1 Condition 1

Let $\mathcal{C}_1$, $\mathcal{C}_2$ and $\mathcal{C}_3$ be the sets of reachable positions respectively by S_1, S_2 and S_3 for a given position and orientation of the platform. Therefore, $\mathcal{C}_1$ and $\mathcal{C}_3$ describe circles and $\mathcal{C}_2$ a circular arc, whose respective centres are the vertices of the platform and the respective radii the length of the proximal links l_i.

From a design standpoint, a necessary and sufficient condition to avoid a singularity of matrix $\boldsymbol{J}_z$ can be formulated as follows: no line intersects $\mathcal{C}_1$, $\mathcal{C}_2$ and $\mathcal{C}_3$. This condition is illustrated in Fig. 7. The shaded area is the set of all lines intersecting both $\mathcal{C}_1$ and $\mathcal{C}_3$. This area is delimited by the common tangent lines to $\mathcal{C}_1$ and $\mathcal{C}_3$. If $\mathcal{C}_2$ does not intersect this area, then $\boldsymbol{J}_z$ is never singular.

Note that this condition is only a consideration that can be taken into account during the design, and is neither necessary nor sufficient for the feasibility of the unlimited rotation problem. Indeed, even if a line can intersect $\mathcal{C}_1$, $\mathcal{C}_2$ and $\mathcal{C}_3$, there is no guarantee that a singular configuration will happen since the value of ψ_3 is not free and is rather obtained from ψ_1 and ψ_2. Moreover, this condition does not prevent the singularity of matrix $\boldsymbol{J}_u$.

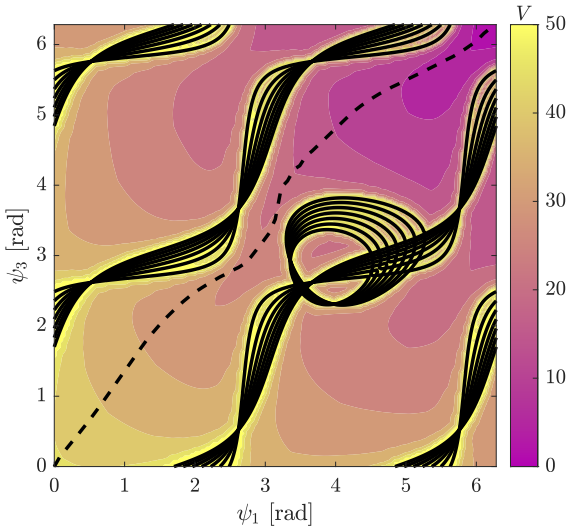

Fig. 8. Feasibility test by path planning.

6.2 Condition 2

If there is a periodic trajectory $\psi_3(\psi_1)$ with period 2π performing a complete rotation for any value of $\psi_2 \in [\underline{\psi}_2, \overline{\psi}_2]$, then the unlimited rotation is feasible. This can be tested in simulation using the path planning method from Section 5 by discretizing $[\underline{\psi}_2, \overline{\psi}_2]$.

Simulation results using the same platform as in Section 5 with $[\underline{\psi}_2, \overline{\psi}_2] = \left[\frac{\pi}{3} - \frac{\pi}{8}, \frac{\pi}{3} + \frac{\pi}{8}\right]$, $\Delta\psi_1 = \frac{\pi}{36}$, $\lambda = 5$ and $\varepsilon = 0.04$ are shown in Fig. 8. In this case, the path generation succeeded. Therefore, the unlimited rotation problem is feasible with $\psi_2 \in [\underline{\psi}_2, \overline{\psi}_2]$. However, situations in which path planning fails are not necessarily infeasible since (i) ψ_2 does not take different values at the same time and (ii) local minima may prevent the gradient descent to succeed close to singularities.

7 DESIGN CONSIDERATIONS

This section discusses the design of the platform in order to reduce the actuation forces.

A platform can be considered as a set of ten independent parameters

$$\rho = (L_i, l_i, \phi_2, \phi_3, \underline{\psi}_2, \overline{\psi}_2) \tag{24}$$

with $i \in \{1, 2, 3\}$. Then, the singularity index $\mathcal{I}_d$ is a

function of ψ_1, ψ_2, ψ_3 and ρ: $\mathcal{I}_d = \mathcal{I}_d(\psi_1, \psi_2, \psi_3, \rho)$.

Let $\mathbb{P}$ be the set of all platforms. The performance index $\mathcal{M}$ of a platform $\rho \in \mathbb{P}$ is defined as the lowest value of $\mathcal{I}_d$ for any value of ψ_1 and ψ_2, where the value of ψ_3 maximizes $\mathcal{I}_d$ for a given ψ_1 and ψ_2. Hence,

$$\mathcal{M}(\rho) = \min_{\psi_1,\psi_2} \mathcal{I}_d(\psi_1, \psi_2, \psi_3, \rho) \tag{25}$$

subject to the constraint

$$\psi_3 = \arg\max_{\psi_3} \mathcal{I}_d(\psi_1, \psi_2, \psi_3, \rho). \tag{26}$$

Practically speaking, the number of free parameters to optimize is much lower than ten. The design is illustrated with an example. Figure 9 shows a gripper whose opening and orientation can be controlled with the redundant links R_iS_i. Here, angle ψ_1 controls the orientation of the gripper and angle ψ_2 the opening through springs and a wire transmission. The timing belt with ratio 3:1 guarantees a 180° rotation of the gripper in configurations where unlimited rotation is prevented due to mechanical interference between the configurable platform and the legs. The configurable platform is attached to the leg mechanisms using spherical joints proposed by Schreiber and Gosselin [8]. These joints use a kinematically redundant design and generate a very large range of motion, exceeding ±150°. The CAD model suggests that L_i is at least 8×10^{-2} m and l_i at most 6×10^{-2} m to avoid interference between redundant links R_iS_i. The range of motion of angle ψ_2 is $\overline{\psi}_2 - \underline{\psi}_2 = 60°$ (modulo 360°). Therefore, the only parameters to optimize are ψ_2, ϕ_3 and $\underline{\psi}_2$ (or, equivalently, $\overline{\psi}_2$).

In order to reduce the computational complexity, the approach is separated in two steps. First, the optimal value for $\underline{\psi}_2$ is obtained considering initially an equilateral triangle as the platform. Then, the platform is optimized with respect to ϕ_2 and ϕ_3. The impact of $\underline{\psi}_2$ is illustrated in Figure 10. The shaded area in Fig. 7 shows the optimal interval $[\underline{\psi}_2, \overline{\psi}_2]$, and the circle in Fig. 7 is the optimal value for $\underline{\psi}_2$. Figure 11 shows the impact of ϕ_2 and ϕ_3 on the performance index $\mathcal{M}$. It can be seen that $\phi_2 = \frac{2\pi}{3}$ and $\phi_3 = \frac{4\pi}{3}$, corresponding to an equilateral triangle, are the optimal values. The video accompanying this paper shows an animation of the CAD model performing unlimited rotations. The robot used for the simulations is designed by our research group [27]. It can be seen that there is no mechanical interference.

Note that if the lengths L_i and l_i are not identical, the optimal values for ϕ_2 and ϕ_3 are different. Figure 12 shows the effect of ϕ_2 and ϕ_3 with a platform such that: $L_1 = 5 \times 10^{-2}$ m, $L_2 = 6 \times 10^{-2}$ m, $L_3 = 7 \times 10^{-2}$ m, $l_1 = 3 \times 10^{-2}$ m, $l_2 = 4 \times 10^{-2}$ m, $l_3 = 5 \times 10^{-2}$ m. In this case, choosing the optimal values rather than $\phi_2 = \frac{2\pi}{3}$ and $\phi_3 = \frac{4\pi}{3}$ yields a 0.9% improvement of the performance index, which may nevertheless not be that significant in practice.

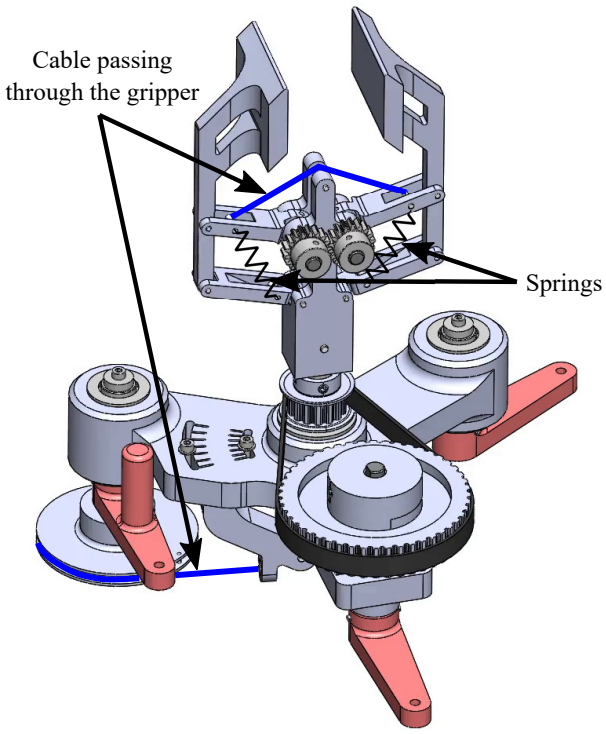

Fig. 9. CAD model of the gripper.

8 OTHER PLATFORMS

There are three categories of planar platforms combining P (prismatic) and R (revolute) joints for unlimited rotations, namely: 3R (three revolute), 1P2R (one prismatic and two revolute) and 2P1R (two prismatic and one revolute). Platform 3R has been studied above. In the following, platforms 1P2R and 2P1R are discussed.

8.1 Platform 1P2R

Platform 1P2R uses a parameterization similar to the one used for platform 3R. Some geometric parameters specific to the platform 1P2R are shown in Fig. 13. The axis of the prismatic joint is $(T_3, \boldsymbol{v}_3)$, with $\boldsymbol{v}_3 = \cos(\phi_3 + \psi_3)\boldsymbol{x}_b + \sin(\phi_3 + \psi_3)\boldsymbol{y}_b$. Parameter r is defined such that $\boldsymbol{s}_3 = \boldsymbol{t}_3 + r\boldsymbol{v}_3$. It should be pointed

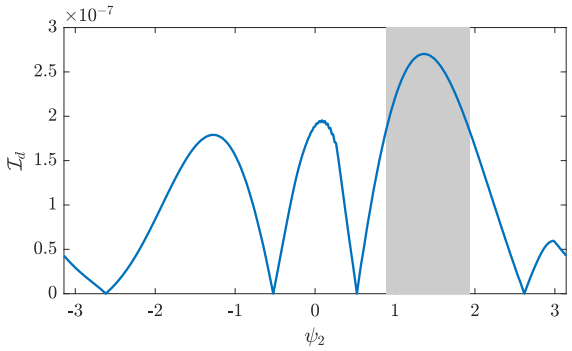

(a) Worst-case value of $\mathcal{I}_d$ as a function of ψ_2

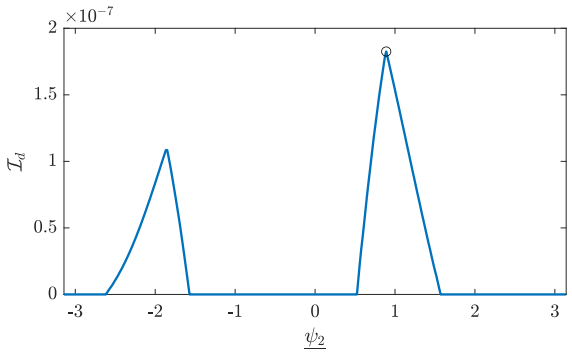

(b) Effect of $\underline{\psi_2}$ on $\mathcal{I}_d$

Fig. 10. Impact of $\underline{\psi_2}$ on $\mathcal{I}_d$. The shaded area corresponds to the optimal $[\underline{\psi_2}, \overline{\psi_2}]$.

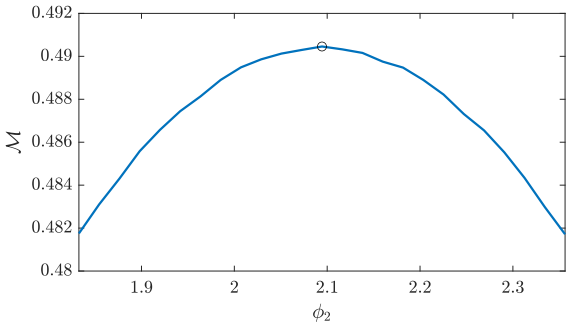

(a) Performance index $\mathcal{M}$ as a function of ϕ_2

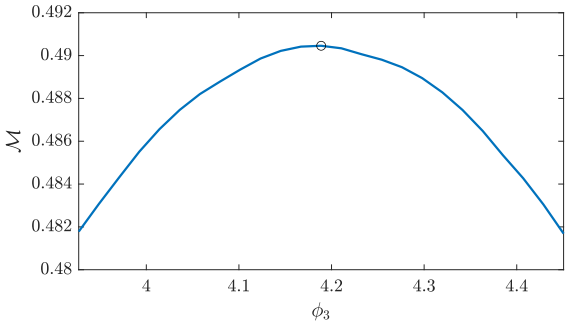

(b) Performance index $\mathcal{M}$ as a function of ϕ_3

Fig. 11. Performance index $\mathcal{M}$ as a function of ϕ_2 and ϕ_3 with $L_i = L$ and $l_i = l$. The circles show the initial guess.

out that for this platform, ψ_3 is a constant design parameter.

Let ξ_{P_r} be the twist of the prismatic joint. Then,

$$\xi_{EE} = \xi_{P_3} + \xi_{S_3} + \xi_{P_r}. \tag{27}$$

Let $\boldsymbol{v}_{3\perp}$ be a unit vector such that ${\boldsymbol{v}_3}^T \boldsymbol{v}_{3\perp} = 0$ and $\boldsymbol{v}_3 \times \boldsymbol{v}_{3\perp} = \boldsymbol{z}_b$. Then, the zero-pitch twist $\xi_{S_3,\boldsymbol{v}_{3\perp}}$ of line $(S_3, \boldsymbol{v}_{3\perp})$ is reciprocal to ξ_{S_3} and ξ_{P_r}. Hence,

$$\xi_{S_3,\boldsymbol{v}_{3\perp}} \cdot \xi_{EE} = \xi_{S_3,\boldsymbol{v}_{3\perp}} \cdot \xi_{P_3} \tag{28}$$

which gives

$${\boldsymbol{v}_{3\perp}}^T \dot{\boldsymbol{p}} + (\boldsymbol{s}_3 \times \boldsymbol{v}_{3\perp})^T \boldsymbol{\omega} = {\boldsymbol{v}_{3\perp}}^T \dot{\boldsymbol{s}}_3. \tag{29}$$

Combining (4), (6) and (29) yields

$$\begin{bmatrix} {\boldsymbol{u}_1}^T & (\boldsymbol{t}_1 \times \boldsymbol{u}_1)^T \\ {\boldsymbol{u}_2}^T & (\boldsymbol{t}_2 \times \boldsymbol{u}_2)^T \\ {\boldsymbol{v}_{3\perp}}^T & (\boldsymbol{s}_3 \times \boldsymbol{v}_{3\perp})^T \\ {\boldsymbol{z}_b}^T & (\boldsymbol{s}_1 \times \boldsymbol{z}_b)^T \\ {\boldsymbol{z}_b}^T & (\boldsymbol{s}_2 \times \boldsymbol{z}_b)^T \\ {\boldsymbol{z}_b}^T & (\boldsymbol{s}_3 \times \boldsymbol{z}_b)^T \end{bmatrix} \begin{bmatrix} \dot{\boldsymbol{p}} \\ \boldsymbol{\omega} \end{bmatrix} = \begin{bmatrix} {\boldsymbol{u}_1}^T & \boldsymbol{0}^T & \boldsymbol{0}^T \\ \boldsymbol{0}^T & {\boldsymbol{u}_2}^T & \boldsymbol{0}^T \\ \boldsymbol{0}^T & \boldsymbol{0}^T & {\boldsymbol{v}_{3\perp}}^T \\ {\boldsymbol{z}_b}^T & \boldsymbol{0}^T & \boldsymbol{0}^T \\ \boldsymbol{0}^T & {\boldsymbol{z}_b}^T & \boldsymbol{0}^T \\ \boldsymbol{0}^T & \boldsymbol{0}^T & {\boldsymbol{z}_b}^T \end{bmatrix} \begin{bmatrix} \dot{\boldsymbol{s}}_1 \\ \dot{\boldsymbol{s}}_2 \\ \dot{\boldsymbol{s}}_3 \end{bmatrix}. \tag{30}$$

The singularity analysis is similar to that of the platform with three R joints studied above. Since $\boldsymbol{s}_3 \times \boldsymbol{v}_{3\perp}$ has no component along $\boldsymbol{z}_b$, type II singularities happen if and only if either $\boldsymbol{J}_z$ (10) or $\boldsymbol{J}_v$ is singular, with

$$\boldsymbol{J}_v = \begin{bmatrix} {\boldsymbol{u}_1}^T \boldsymbol{x}_b & {\boldsymbol{u}_1}^T \boldsymbol{y}_b & (\boldsymbol{t}_1 \times \boldsymbol{u}_1)^T \boldsymbol{z}_b \\ {\boldsymbol{u}_2}^T \boldsymbol{x}_b & {\boldsymbol{u}_2}^T \boldsymbol{y}_b & (\boldsymbol{t}_2 \times \boldsymbol{u}_2)^T \boldsymbol{z}_b \\ {\boldsymbol{v}_{3\perp}}^T \boldsymbol{x}_b & {\boldsymbol{v}_{3\perp}}^T \boldsymbol{y}_b & (\boldsymbol{s}_3 \times \boldsymbol{v}_{3\perp})^T \boldsymbol{z}_b \end{bmatrix}. \tag{31}$$

From Grassmann line geometry, matrix $\boldsymbol{J}_v$ is singular if and only if lines $(S_1, \boldsymbol{u}_1)$, $(S_2, \boldsymbol{u}_2)$ and $(S_3, \boldsymbol{v}_{3\perp})$ have a common intersection or are parallel to each other.

Consider a platform with the following parameters: $L_1 = L_2 = 8 \times 10^{-2}$ m, $L_3 = 0$, $l_1 = l_2 = 7.3 \times 10^{-2}$ m,

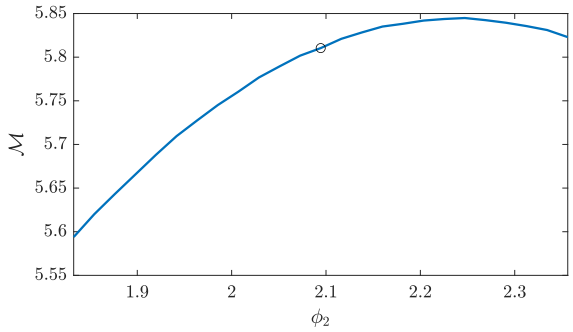

(a) Performance index $\mathcal{M}$ as a function of ϕ_2

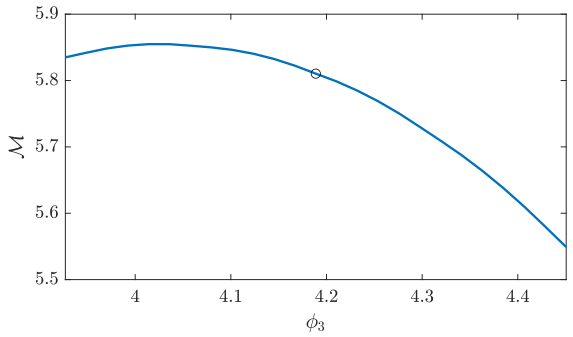

(b) Performance index $\mathcal{M}$ as a function of ϕ_3

Fig. 12. Effect of ϕ_2 and ϕ_3 on the performance index $\mathcal{M}$ for an asymmetrical platform. The circles show the initial guess.

$\phi_1 = 0$, $\phi_2 = \frac{2\pi}{3}$, $\phi_3 = \frac{4\pi}{3}$, $\psi_3 = 0$ and $[\underline{r}_3, \overline{r}_3] = [0.05,\ 0.1]$. The potential $V(\psi_1, \psi_2)$ for $r_3 \in [\underline{r}_3, \overline{r}_3]$ with the initial point $\psi_1 = \psi_2 = 0$ is shown in Fig. 14. As it can be seen, unlimited rotation is feasible without crossing any singularity.

Design considerations presented in Section 7 can also be used for the 1P2R platform. Additionally, parameter ψ_3 needs to be chosen appropriately. Indeed, the effect of ψ_3 on the performance index $\mathcal{M}$ is illustrated in Fig. 15. The value of the performance index is multiplied by 1.6 between $\psi_3 = \frac{\pi}{2}$ (the worst case) and $\psi_3 = 0$ (the best case).

8.2 Platform 2P1R

The parameterization of the 2P1R platform is similar to that of the 1P2R platform. The revolute joint associated with variable ψ_2 is replaced by a prismatic joint of axis $\boldsymbol{v}_3 = \cos(\psi_2 + \psi_2)\boldsymbol{x}_b + \sin(\psi_2 + \psi_2)\boldsymbol{y}_b$ and vector $\boldsymbol{v}_{3\perp}$ is such that $(\boldsymbol{v}_3, \boldsymbol{v}_{3\perp}, \boldsymbol{z}_b)$ is a right-handed orthonormal basis.

The following parameters are defined from Fig. 16. The intersection of lines $(S_1, \boldsymbol{u}_1)$ and $(S_2, \boldsymbol{v}_{2\perp})$ (respectively $(S_3, \boldsymbol{v}_{3\perp})$) is noted M_{12} (respectively M_{13}). Let

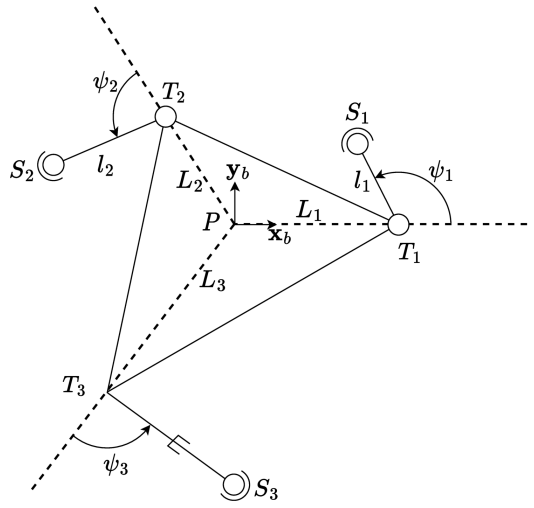

Fig. 13. Parameterization of the platform 1P2R.

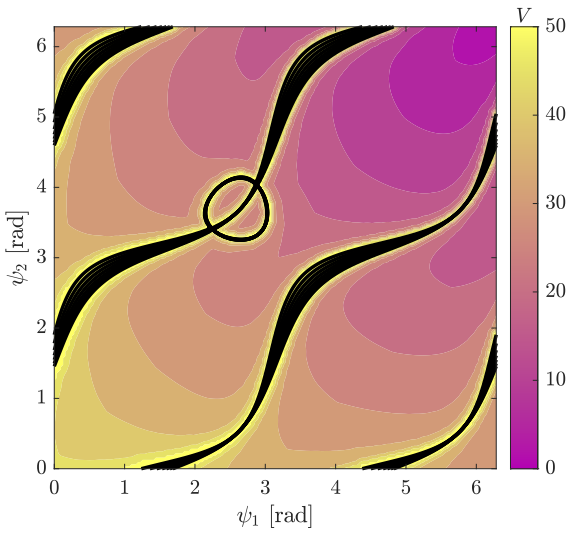

Fig. 14. Potential V for the 1P2R platform.

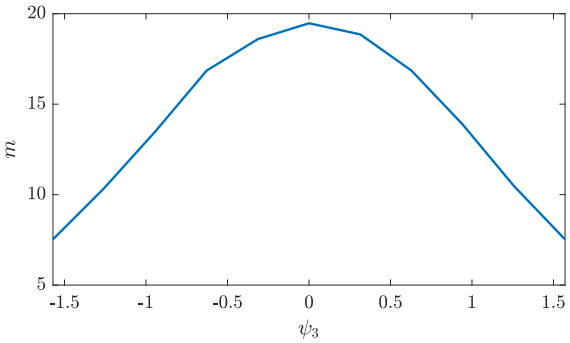

Fig. 15. Effect of ψ_3 on the performance index $\mathcal{M}$ for the 1P2R platform.

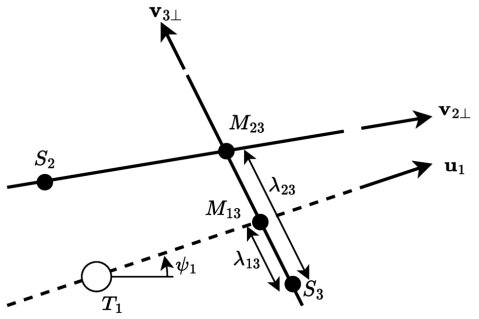

Fig. 16. Parameterization of the platform 2P1R.

$\boldsymbol{m}_{13}$ be the position vector of point M_{13} and $\boldsymbol{m}_{23}$ the position vector of point M_{23}. Parameters λ_{13} and λ_{23} are defined such that $\boldsymbol{m}_{13} = \lambda_{13}\boldsymbol{v}_{3\perp} + \boldsymbol{s}_3$ and $\boldsymbol{m}_{23} = \lambda_{23}\boldsymbol{v}_{3\perp} + \boldsymbol{s}_3$.

According to Grassmann line geometry, the platform is in a singular configuration if lines $(S_1, \boldsymbol{u}_1)$, $(S_2, \boldsymbol{v}_{2\perp})$ and $(S_3, \boldsymbol{v}_{3\perp})$ have a common intersection or are parallel. The case where $\boldsymbol{v}_{2\perp}$ and $\boldsymbol{v}_{3\perp}$ are collinear is not considered since unlimited rotation is trivially unfeasible (there exists a value of ψ_1 such that $\boldsymbol{u}_1$, $\boldsymbol{v}_{2\perp}$ and $\boldsymbol{v}_{3\perp}$ are collinear).

Consider the initial situation of Fig. 16, in which $\lambda_{13} < \lambda_{23}$ and $\dot{\psi}_1 > 0$. The case $\lambda_{13} > \lambda_{23}$ is equivalent to this one considering a rotation of ψ_1 in the opposite direction, i.e., $\dot{\psi}_1 < 0$. Let ψ_o be the initial value of ψ_1 and $\psi_f > \psi_o$ be the value of ψ_1 such that $(S_1, \boldsymbol{u}_1)$ is parallel to $(S_3, \boldsymbol{v}_{3\perp})$ and ${\boldsymbol{u}_1}^T\boldsymbol{v}_{3\perp} > 0$.

We now show that unlimited rotation of ψ_1 is not feasible for constant r_3 using a proof by contradiction. If unlimited rotation of ψ_1 is feasible, then ψ_1 can move from ψ_o to ψ_f. Let $f : [\psi_o, \psi_f] \to \mathbb{R}$ be a continuous function associating to each value of ψ_1 a feasible value of λ_{23}. In other words, f is a feasible path for M_{23}. The existence of such a function is guaranteed since it is necessary for unlimited rotation. Since f is continuous, there exists a segment (a closed and bounded interval) $[\underline{\lambda}_{23}, \overline{\lambda}_{23}]$ such that $[\underline{\lambda}_{23}, \overline{\lambda}_{23}] = f([\psi_o, \psi_f])$. However, λ_{13} goes to $+\infty$ when ψ_1 converges towards ψ_f. Since $\lambda_{23} > \lambda_{13}$, interval $[\underline{\lambda}_{23}, \overline{\lambda}_{23}]$ cannot be bounded, which is contradictory. Indeed, moving ψ_1 from ψ_o to ψ_f is assumed to be feasible. As a consequence, unlimited rotation is not feasible. Note that the same reasoning can be applied to the platform 1P2R if ψ_2 is constant and r_3 is used to avoid singularities.

9 CONCLUSION AND PERSPECTIVES

With appropriate design and initial configuration, the planar platform of a $(6 + 3)$-DoF tripedal parallel robot can carry out unlimited rotation if it is equipped with at least two revolute joints (and at most one prismatic joint). A method based on artificial potential fields is proposed in order to find a feasible path for unlimited rotation. The success of the path finding approach can also be used as a sufficient condition for the feasibility of the unlimited rotation problem. Two singularity indices are compared in order to resolve the redundancy while reducing the actuated joint torques. A performance index based on a singularity index is proposed and the impact of geometric parameters are discussed in order to identify rules for the design of the platform. While the presented methods are applied to determine the architecture parameters that can produce unlimited rotation, they can also be used for tasks requiring a smaller (finite) range of motion.

An immediate perspective to this work is the generalization to spatial platforms. Therefore, any 3-DoF parallel mechanism could be used as a configurable platform without requiring transmission components. As an example, it could be possible to have three revolute joints with concurrent axes in order to produce a spherical movement [28].

ACKNOWLEDGEMENTS

This work was supported by the Natural Sciences and Engineering Research Council of Canada (NSERC).

REFERENCES

[1] Gosselin, C., and Schreiber, L.-T., 2018, "Redundancy in Parallel Mechanisms: A Review," *Applied Mechanics Reviews,* **70**(1).

[2] Schreiber, L.-T., and Gosselin, C., 2019, "Schönflies Motion PARAllel Robot (SPARA): A Kinematically Redundant Parallel Robot With Unlimited Rotation Capabilities," *IEEE/ASME Transactions on Mechatronics,* **24**(5), pp. 2273–2281.

[3] Company, O., Pierrot, F., Nabat, V., and de la O Rodriguez, M., 2005, "Schoenflies Motion Generator: A New Non Redundant Parallel Manipulator with Unlimited Rotation Capability," In Proceedings of the IEEE International Conference on Robotics and Automation, pp. 3250–3255.

[4] Gosselin, C., Isaksson, M., Marlow, K., and Laliberté, T., 2016, "Workspace and Sensitivity Analysis of a Novel Nonredundant Parallel SCARA Robot

Featuring Infinite Tool Rotation," *IEEE Robotics and Automation Letters,* **1**(2), 7, pp. 776–783.

[5] Babin, V., and Gosselin, C., 2018, "Picking, grasping, or scooping small objects lying on flat surfaces: A design approach," *The International Journal of Robotics Research,* **37**(12), pp. 1484–1499.

[6] Gosselin, C., Laliberté, T., and Veillette, A., 2015, "Singularity-Free Kinematically Redundant Planar Parallel Mechanisms With Unlimited Rotational Capability," *IEEE Transactions on Robotics,* **31**(2), pp. 457–467.

[7] Gosselin, C., and Schreiber, L.-T., 2016, "Kinematically Redundant Spatial Parallel Mechanisms for Singularity Avoidance and Large Orientational Workspace," *IEEE Transactions on Robotics,* **32**(2), pp. 286–300.

[8] Schreiber, L.-T., and Gosselin, C., 2017, "Passively Driven Redundant Spherical Joint With Very Large Range of Motion," *ASME Journal of Mechanisms and Robotics,* **9**(3).

[9] Stepanenko, O., Bonev, I. A., and Zlatanov, D., 2019, "A New 4-DOF Fully Parallel Robot With Decoupled Rotation for Five-Axis Micromachining Applications," *Journal of Mechanisms and Robotics,* **11**(3).

[10] Wen, K., Nguyen, T. S., Harton, D., Laliberté, T., and Gosselin, C., 2021, "A Backdrivable Kinematically Redundant (6+3)-Degree-of-Freedom Hybrid Parallel Robot for Intuitive Sensorless Physical Human-Robot Interaction," *IEEE Transactions on Robotics,* **37**(4), pp. 1222–1238.

[11] Luces, M., Mills, J. K., and Benhabib, B., 2017, "A Review of Redundant Parallel Kinematic Mechanisms," *Journal of Intelligent & Robotic Systems,* **86**(2), pp. 175–198.

[12] Wen, K., and Gosselin, C., 2019, "Kinematically Redundant Hybrid Robots With Simple Singularity Conditions and Analytical Inverse Kinematic Solutions," *IEEE Robotics and Automation Letters,* **4**(4), pp. 3828–3835.

[13] Siciliano, B., 1990, "Kinematic control of redundant robot manipulators: A tutorial," *Journal of Intelligent and Robotic Systems,* **3**(3), pp. 201–212.

[14] Yoshikawa, T., 1985, "Manipulability and redundancy control of robotic mechanisms," In Proceedings of the IEEE International Conference on Robotics and Automation, Vol. 2, pp. 1004–1009.

[15] Klein, C. A., and Blaho, B. E., 1987, "Dexterity Measures for the Design and Control of Kinematically Redundant Manipulators," *The International Journal of Robotics Research,* **6**(2), pp. 72–83.

[16] Liégeois, A., 1977, "Automatic Supervisory Control of the Configuration and Behavior of Multibody Mechanisms," *IEEE Transactions on Systems, Man, and Cybernetics,* **7**(12), pp. 868–871.

[17] Voglewede, P., and Ebert-Uphoff, I., 2004, "Measuring "closeness" to singularities for parallel manipulators," In Proceedings of the IEEE International Conference on Robotics and Automation, pp. 4539–4544.

[18] Wolf, A., and Shoham, M., 2003, "Investigation of Parallel Manipulators Using Linear Complex Approximation," *Journal of Mechanical Design,* **125**(3), pp. 564–572.

[19] Hesselbach, J., Bier, C., Campos, A., and Lowe, H., 2005, "Direct Kinematic Singularity Detection of a Hexa Parallel Robot," In Proceedings of the IEEE International Conference on Robotics and Automation, pp. 3238–3243.

[20] Chang, W.-T., Lin, C.-C., and Lee, J.-J., 2003, "Force Transmissibility Performance of Parallel Manipulators," *Journal of Robotic Systems,* **20**(11), pp. 659–670.

[21] Liu, X.-J., Wu, C., and Wang, J., 2012, "A New Approach for Singularity Analysis and Closeness Measurement to Singularities of Parallel Manipulators," *Journal of Mechanisms and Robotics,* **4**(4).

[22] Cardou, P., Bouchard, S., and Gosselin, C., 2010, "Kinematic-Sensitivity Indices for Dimensionally Nonhomogeneous Jacobian Matrices," *IEEE Transactions on Robotics,* **26**(1), 2, pp. 166–173.

[23] Crameri, F., 2021, Scientific colour maps.

[24] Min Cheol Lee, and Min Gyu Park, 2003, "Artificial potential field based path planning for mobile robots using a virtual obstacle concept," In Proceedings of the IEEE/ASME International Conference on Advanced Intelligent Mechatronics, pp. 735–740.

[25] Barraquand, J., and Latombe, J.-C., 1990, "A Monte-Carlo algorithm for path planning with many degrees of freedom," In Proceedings of the IEEE International Conference on Robotics and Automation, IEEE Comput. Soc. Press, pp. 1712–1717.

[26] Tsardoulias, E. G., Iliakopoulou, A., Kargakos, A., and Petrou, L., 2016, "A Review of Global Path Planning Methods for Occupancy Grid Maps Regardless of Obstacle Density," *Journal of Intelligent & Robotic Systems,* **84**(1-4), pp. 829–858.

[27] Yigit, A., Breton, D., Zhou, Z., Laliberté, T., and Gosselin, C., 2023, "Kinematic Analysis and Design of a Novel (6+3)-DoF Parallel Robot with Fixed Actuators," In Proceedings of the IEEE International Conference on Robotic and Automation.

[28] Gosselin, C., and Hamel, J.-F., 1994, "The agile eye: a high-performance three-degree-of-freedom

camera-orienting device," In Proceedings of the IEEE International Conference on Robotics and Automation, pp. 781–786.